

DISEASES AND DISORDERS

Epidermal autonomous VEGFA/Flt1/Nrp1 functions mediate psoriasis-like disease

Farida Benhadou^{1,2}, Elisabeth Gitzner³, Audrey Brisebarre¹, Benjamin Swedlund¹, Yura Song¹, Christine Dubois¹, Milena Rozzi¹, Catherine Paulissen¹, Veronique del Marmol², Maria Sibilia³, Cédric Blanpain^{1,4*}

Psoriasis is a common chronic skin disorder characterized by keratinocyte hyperproliferation with altered differentiation accompanied by inflammation and increased angiogenesis. It remains unclear whether the first events that initiate psoriasis development occur in keratinocytes or inflammatory cells. Here, using different psoriasis mouse models, we showed that conditional deletion of *Flt1* or *Nrp1* in epidermal cells inhibited psoriasis mediated by *Vegfa* overexpression or *c-Jun/JunB* deletion. Administration of anti-Nrp1 antibody reverted the psoriasis phenotype. Using transcriptional and chromatin profiling of epidermal cells following *Vegfa* overexpression together with *Flt1* or *Nrp1* deletion, we identified the gene regulatory network regulated by *Vegfa/Nrp1/Flt1* during psoriasis development and uncovered a key role of *Fosl1* in regulating the chromatin remodeling mediated by *Vegfa* overexpression in keratinocytes. In conclusion, our study identifies an epidermal autonomous function of *Vegfa/Nrp1/Flt1* that mediates psoriatic-like disease and demonstrates the clinical relevance of blocking *Vegfa/Nrp1/Flt1* axis in psoriasis.

INTRODUCTION

Psoriasis is a frequent skin inflammatory disorder affecting approximately 3% of the world population (1). Psoriasis vulgaris is the most common type and is characterized by erythematous and scaly plaques of the skin. Psoriasis vulgaris typically occurs in the elbows, knees, or scalp regions. In addition to the skin lesions, several other organs can be affected in psoriasis, including arthritis, metabolic syndrome, or bowel inflammatory disease, which all contribute to the disease burden (1). Histologically, psoriasis is characterized by a hyper-thickening of the skin epidermis with increased vascularization and immune infiltration of the dermis (2). Although psoriasis is an autoimmune disease, the skin epidermis is also an important player in the initial pathogenesis of psoriasis and contributes to the recruitment of inflammatory cells, and the cross-talk between epidermal cells and immune cells is likely to be important for the pathogenesis of psoriasis (2).

Vascular endothelial growth factor A (VEGFA), the main pro-angiogenic factor, is overexpressed in human psoriasis skin and is correlated to disease severity (3). A role for VEGFA in psoriasis was suggested by *VEGFA* genomic location in close proximity to *PSORS1*, one of the psoriasis susceptibility loci, and the correlation of single nucleotide polymorphism in *VEGFA* with psoriasis severity (4). Administration of bevacizumab, a monoclonal antibody targeting VEGFA, for the treatment of solid cancers has been associated with improvement of psoriatic lesions (5). Experimental studies also demonstrated the effectiveness of VEGFA blocking therapy in improving the skin phenotype in mouse models of psoriasis-like disease (6–8).

Transgenic mouse models overexpressing *Vegfa* in keratinocytes lead to the development of an inflammatory skin condition recapitulating the main hallmarks of human psoriasis, supporting a key role of *Vegfa* expressed by keratinocytes in promoting psoriasis-like disease

(8–10). However, the precise roles played by VEGFA in mediating psoriasis are poorly understood. VEGFA mediates its effects by binding to tyrosine kinase receptors Flt1 (VEGFR1) and Flk1 (VEGFR2) (11). Neuropilin 1 (Nrp1) acts as a VEGFA coreceptor amplifying VEGFA signaling by promoting VEGFR receptor signaling in the same cells (cis effect) or presenting VEGFA to neighboring cells (trans effect) (12).

Despite the well-known role of VEGFA in psoriasis, the molecular mechanism by which VEGFA promotes psoriasis is not well understood. It remains unclear on which cells VEGFA acts to promote psoriasis and the molecular mechanisms downstream of VEGFA in this process. Does VEGFA act only on blood vessels or macrophages, as it has been previously suggested (13), which in turn mediates recruitment of inflammatory cells and causes the defect of keratinocyte differentiation, or does VEGFA also act directly on epidermal cells in an autocrine or a paracrine manner to orchestrate the changes associated with psoriasis, as it has been suggested during tumorigenesis (14, 15)?

Using genetically engineered psoriasis mouse models, we assessed the role of Nrp1 or Flt1 expression by epidermal cells to induce psoriasis development in a cell autonomous manner. Unexpectedly, we found that deletion of *Nrp1* or *Flt1* in the skin epidermis completely prevents the development of psoriasis following *Vegfa* overexpression. In addition, epidermal deletion of *Flt1* in mice with *c-Jun/JunB* deletion, one of the best-studied mouse models of psoriasis (16), also leads to a notable improvement of the psoriasis lesions. We showed that therapeutic administration of Nrp1-blocking antibodies reverts the development of psoriatic lesions induced by *Vegfa*.

Combination of RNA sequencing (RNA-seq) and assay for transposase-accessible chromatin sequencing (ATAC-seq) on fluorescence-activated cell sorting (FACS)-isolated epidermal cells following *Vegfa* overexpression in the presence or in the absence of *Flt1* or *Nrp1* allowed the identification of the gene regulatory network downstream of Flt1/Nrp1 in keratinocytes that control the development of *Vegfa*-induced psoriasis. Together, our results unravel a novel cell autonomous function of Flt1 and Nrp1 in epidermal cells that promotes *Vegfa*-induced psoriasis and opens

Copyright © 2020
The Authors, some
rights reserved;
exclusive licensee
American Association
for the Advancement
of Science. No claim to
original U.S. Government
Works. Distributed
under a Creative
Commons Attribution
NonCommercial
License 4.0 (CC BY-NC).

Downloaded from <http://advances.sciencemag.org/> on January 9, 2020

¹Laboratory of Stem Cells and Cancer, Université Libre de Bruxelles, Brussels, Belgium. ²Dermatology Department, Erasme Hospital, Université Libre de Bruxelles, Brussels, Belgium. ³Institute of Cancer Research, Department of Medicine I, Medical University of Vienna and Comprehensive Cancer Center, Vienna, Austria. ⁴WELBIO, Université Libre de Bruxelles, Brussels B-1070, Belgium.

*Corresponding author. Email: cedric.blanpain@ulb.ac.be

the way for new therapeutic opportunities for the treatment of psoriatic disease.

RESULTS

Epidermal autonomous expression of *Flt1* is essential for psoriasis development induced by *Vegfa*

As previously reported, *Vegfa* overexpression in mouse epidermis using K14-Cre/Rosa-*Vegfa* (K14-*Vegfa*) induces a psoriatic-like disease (8), which appears 1 month postnatally and characterized macroscopically by red skin, scaly lesions in the ear and the tail, as well as severe erythema and edema of the oral mucosa (fig. S1, A and B), and microscopically by hyperplasia of the epidermis, abnormal keratinocyte differentiation, increase in epidermal cell proliferation, immune infiltration, and blood vessel density (fig. S1, C to J). These macroscopic and microscopic features represent the hallmark of psoriatic skin lesions in humans (17). In this mouse model, different populations of cells express *Vegfa* receptors and coreceptors. Endothelial cells (ECs) express VEGFR2/Flk1 (18), VEGFR1/Flt1 (19), and its coreceptor Nrp1 (20). *Flt1* is also expressed by different immune cells (21), but the *Vegfa* receptors expressed by keratinocytes are still a matter of discussion (22, 23). Nrp1 is a *Vegfa* coreceptor, which promotes *Vegfa* signaling in trans by presenting *Vegfa* to other immune and ECs, or in cis by promoting *Vegfa* signaling in a cell autonomous manner (12). Using RNA-seq or quantitative reverse transcription polymerase chain reaction (qRT-PCR), we found that basal keratinocytes expressed VEGFR1/Flt1 and Nrp1, but not VEGFR2/Flk1 (fig. S1K).

To assess the cell autonomous role of *Flt1* expression by keratinocytes in *Vegfa*-mediated psoriasis, we deleted *Flt1* exclusively in the epidermis using K14-Cre/Rosa-*Vegfa/Flt1 flox/flox* mice (K14-*Vegfa/Flt1 cKO*) (Fig. 1A). *Vegfa* mRNA expression was comparable in K14-*Vegfa* and K14-*Vegfa/Flt1 cKO* mice (Fig. 1B), whereas *Flt1* expression was virtually abolished at the mRNA and protein levels in K14-*Vegfa/Flt1 cKO* epidermis (Fig. 1, B to D). Epidermal thickness, which was increased by threefold in K14-*Vegfa* epidermis, was normalized to the control level in K14-*Vegfa/Flt1 cKO* epidermis (Fig. 1, F and G).

The hyperplasia of the epidermis in psoriatic skin is associated with increased proliferation of basal keratinocytes (2). Whereas *Vegfa* overexpression increased basal keratinocyte proliferation [51% of EdU (5'-ethynyl-2'-deoxyuridine)-positive cells in K14-*Vegfa* versus 17% for control mice], the deletion of *Flt1* prevented the increase in cell proliferation induced by *Vegfa* (19% of EdU-positive cells) (Fig. 1, H and I).

Psoriatic skin induced by *Vegfa* overexpression is also characterized by an infiltration of immune cells (2). To define whether *Flt1* expression in keratinocytes controls the immune infiltration induced by *Vegfa* overexpression, we performed immunostaining of CD45, a pan-leucocyte marker in the skin epidermis of control, K14-*Vegfa*, and K14-*Vegfa/Nrp1 cKO* mice. *Flt1* deletion in the epidermis completely prevented the increase in dermal immune infiltrate following *Vegfa* overexpression (Fig. 1, J and K). CD19-positive B lymphocytes and F4/80 macrophages were the main immune cell populations increased in the dermis of K14-*Vegfa* mice and were decreased upon epidermal *Flt1* deletion (fig. S2, B and C).

Neovascularization is another important hallmark characterizing psoriatic skin (24). To determine the role of epidermal Nrp1 in the regulation of neovascularization induced by *Vegfa* expression by keratinocytes, we performed CD31 immunostaining in the skin epider-

mis and quantified the microvascular density in the mice expressing or not expressing *Flt1* in the epidermis. Whereas *Vegfa* expression by epidermal cells increased the microvascular density, the deletion of *Flt1* in keratinocytes normalized the microvascular density to the level found in control mice (Fig. 1, L and M).

Epidermal expression of *Nrp1* is required for psoriasis development mediated by *Vegfa*

To investigate whether the expression of Nrp1 by epidermal cells regulates *Vegfa*-mediated psoriasis-like disease, we overexpressed *Vegfa* and deleted *Nrp1* specifically and exclusively in the skin epidermis using K14-Cre/Rosa-*Vegfa/Nrp1 flox/flox* mice (K14-*Vegfa/Nrp1 cKO*) (Fig. 2A). The level of *Vegfa* mRNA expression in basal epidermal cells was comparable between K14-*Vegfa* and K14-*Vegfa/Nrp1 cKO* mice (Fig. 2B), whereas Nrp1 expression was virtually undetectable in the epidermis of K14-*Vegfa/Nrp1 cKO* mice both at the mRNA and protein levels (Fig. 2, B to D). The deletion of *Nrp1* in keratinocytes in K14-*Vegfa/Nrp1 cKO* mice was sufficient to completely block the development of the macroscopic psoriasis phenotype (erythema and scaly skin) in the tail and the ear epidermis induced by *Vegfa* overexpression (Fig. 2E). The deletion of *Nrp1* in the epidermis also prevented the development of microscopic alterations that characterized psoriatic skin, including the epidermal hyperthickening, the increase in basal keratinocyte proliferation, the immune infiltration, and microvascular density associated with *Vegfa* overexpression (Fig. 2, F to I).

The psoriasis-like disease induced by *Vegfa* was unaffected by the deletion of a single allele of either *Nrp1* or *Flt1*, whereas compound heterozygous mice (K14-*Vegfa/Nrp1+/cKO/Flt1+/cKO*) did not present a psoriatic phenotype and were indistinguishable from the complete *Nrp1* or *Flt1 cKO* (fig. S3, A to H), showing that *Flt1* and *Nrp1* interact genetically in an epistatic manner to promote *Vegfa*-induced psoriasis. Together, these data clearly demonstrate the essential cell autonomous function of *Flt1* and *Nrp1* in promoting psoriasis development induced by *Vegfa* overexpression.

Administration of function-blocking anti-Nrp1 antibody improves psoriasis phenotype induced by *Vegfa* overexpression

To assess whether inhibiting Nrp1/*Vegfa* interaction can be of therapeutic relevance for the treatment of psoriasis, we administered to K14-*Vegfa* mice an anti-Nrp1 antibody that blocks the binding of *Vegfa* (Nrp1b antibody) or the binding of semaphorins (Nrp1a antibody) (Fig. 3, A to C) (25, 26).

The epidermal thickness was rapidly normalized following the administration of anti-Nrp1 antibody that blocks Nrp1/*Vegfa* interaction (Fig. 3, D and E). Likewise, keratinocyte hyperproliferation, immune infiltration, and increase in microvascular density induced by *Vegfa* overexpression were also all rapidly normalized following the administration of anti-Nrp1 antibody that blocks *Vegfa* interaction, whereas no improvement of psoriasis was observed after the administration of Nrp1 antibody that blocks semaphorins interaction (Fig. 3, F to K). These data demonstrate the therapeutic benefit of blocking *Vegfa/Nrp1* interaction for the treatment of psoriasis.

Epidermal autonomous expression of *Flt1* is essential for psoriasis development induced by *c-Jun/JunB* deletion

We then assessed whether the essential role of *Flt1* in epidermal cells is conserved across different mouse models of psoriasis. To this

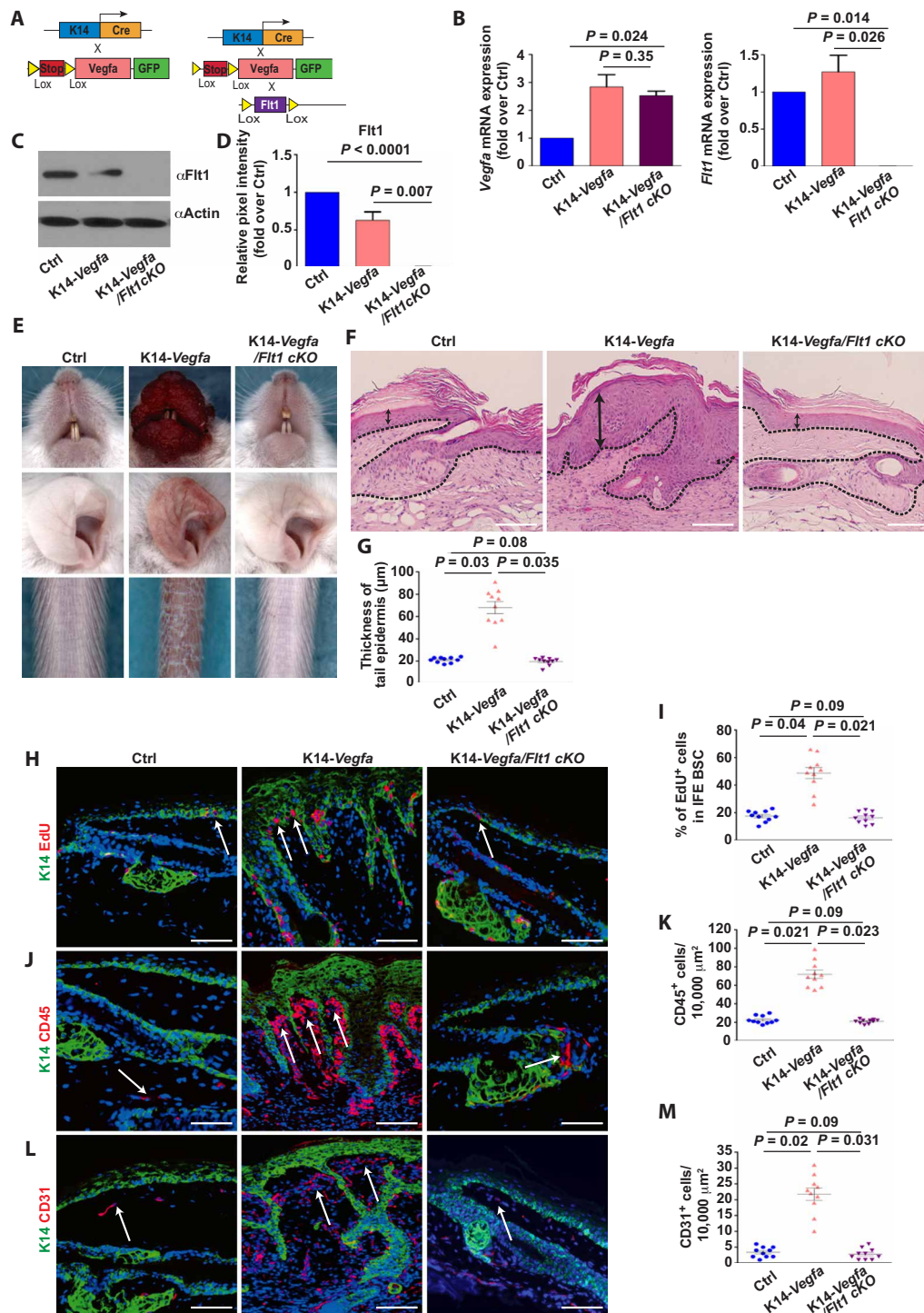


Fig. 1. *Flt1* expression by keratinocytes is essential for *Vegfa*-induced psoriasis. (A) Strategy to constitutively activate *Vegfa* and inhibit *Flt1*. (B) *Vegfa* and *Flt1* mRNA expression by qRT-PCR on FACS-isolated keratinocytes ($n = 3$) (means \pm SEM, Mann-Whitney). (C) *Flt1* expression assessed by Western blot on FACS-isolated basal keratinocytes. (D) *Flt1* protein expression ($n = 3$) (means \pm SEM, Mann-Whitney). (E) Naso-oral region, ear, and tail. (F) Hematoxylin and eosin (H&E) on tail skin. Scale bars, 50 μ m. (G) Epidermal tail thickness measured microscopically ($n = 10$) (means \pm SEM, Student's t test). (H) K14/Edu staining. Scale bars, 50 μ m. (I) Percentage of Edu-positive basal cells (BCs) in interfollicular epidermis (IFE) [$n = 398$ (Ctrl), $n = 436$ (K14-*Vegfa*), $n = 422$ (K14-*Vegfa/Flt1* cKO) total BCs, $n = 10$ mice] (mean \pm SEM, Student's t test). (J) K14/CD45 staining. Scale bars, 50 μ m. (K) Density of CD45-positive cells in dermal IFE area (represents the dermal area just beneath the IFE) of 300,565 μ m² (Ctrl), 289,678 μ m² (K14-*Vegfa*), and 278,767 μ m² (K14-*Vegfa/Flt1* cKO); $n = 10$ mice. Number of CD45-positive cells per 10,000 μ m² (means \pm SEM, Student's t test). (L) K14/CD31 staining. Scale bars, 50 μ m. (M) Number of CD31-positive cells (microvascular density) calculated in dermal IFE area of 324,567 μ m² (Ctrl), 345,234 μ m² (K14-*Vegfa*), and 342,356 μ m² (K14-*Vegfa/Flt1* cKO); $n = 10$ mice. Number of CD31-positive cells per 10,000 μ m² (means \pm SEM, Student's t test). Photo credit: Benhadou Farida, Laboratory of Stem Cells and Cancer.

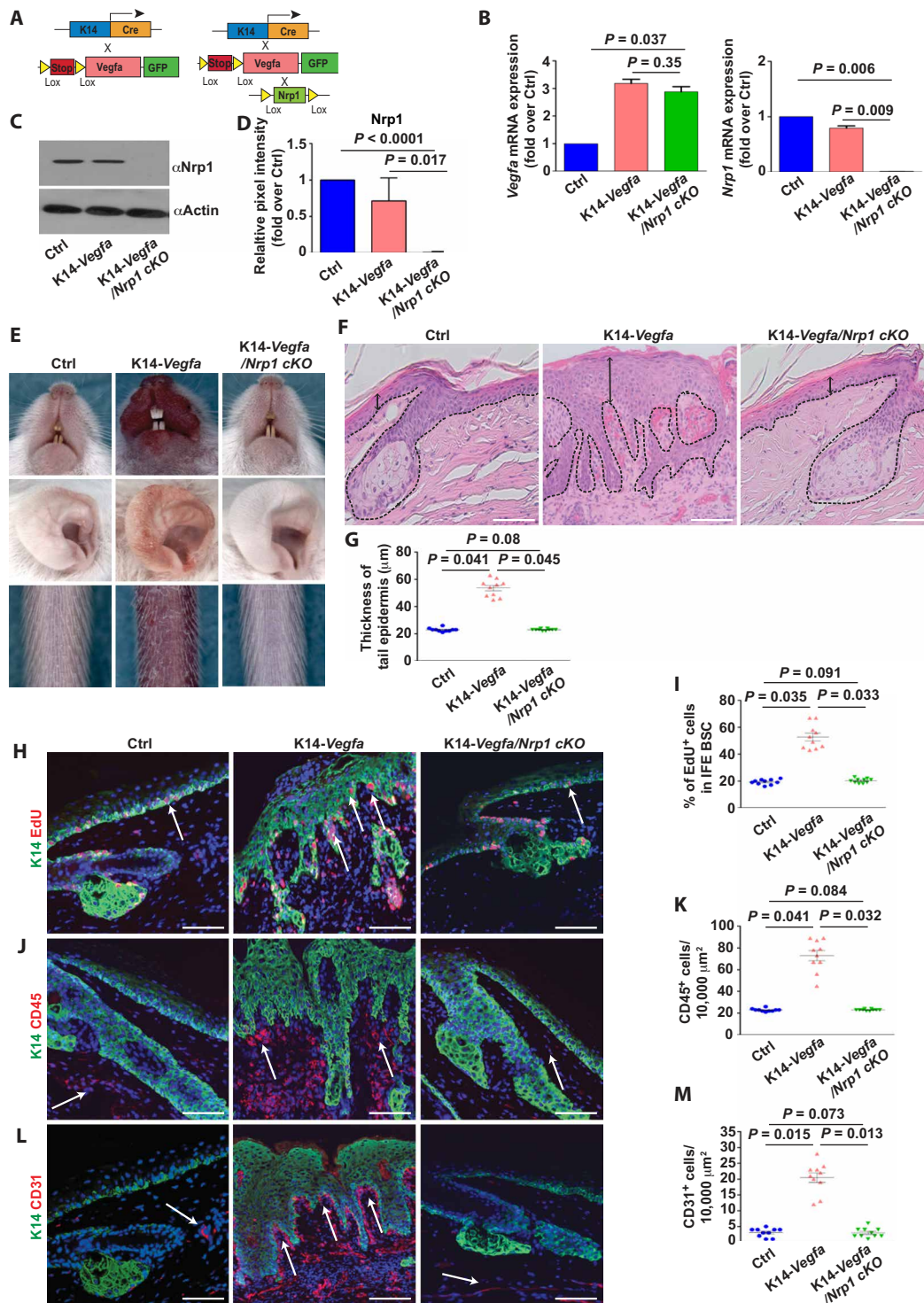


Fig. 2. Cell autonomous function of *Nrp1* in the epidermis is critical for *Vegfa*-induced psoriasis. (A) Strategy to constitutively activate *Vegfa* and delete *Nrp1* expression in epidermis. (B) *Vegfa* and *Nrp1* mRNA expression by qRT-PCR on FACS-isolated keratinocytes ($n = 3$) (means \pm SEM, Mann-Whitney test). (C) *Nrp1* expression assessed by Western blot performed on FACS-isolated basal keratinocytes. (D) *Nrp1* protein expression ($n = 3$) (means \pm SEM, Mann-Whitney test). (E) Naso-oral region, ear, and tail. (F) H&E on tail skin. Scale bars, 50 μm . (G) Epidermal tail thickness measured microscopically ($n = 10$) (mean \pm SEM, Student's t test). (H) K14/EdU staining. Scale bars, 50 μm . (I) Percentage of EdU-positive BCs [$n = 507$ (Ctrl), $n = 487$ (K14-Vegfa), $n = 490$ (K14-Vegfa/*Nrp1* cKO) total BCs; $n = 10$ mice] (means \pm SEM, Student's t test). (J) K14/CD45 staining. Scale bars, 50 μm . (K) Density of CD45-positive cells in the dermal IFE area of 344,965 μm^2 (Ctrl), 449,687 μm^2 (K14-Vegfa), and 423,876 μm^2 (K14-Vegfa/*Nrp1* cKO); $n = 10$ mice. CD45-positive cells per 10,000 μm^2 (means \pm SEM, Student's t test). (L) K14/CD31 staining. Scale bars, 50 μm . (M) Number of CD31-positive cells calculated in a dermal IFE area of 409,560 μm^2 (Ctrl), 432,890 μm^2 (K14-Vegfa), and 428,532 μm^2 (K14-Vegfa/*Nrp1* cKO); $n = 10$ mice. Number of CD31-positive cells per 10,000 μm^2 (means \pm SEM, Student's t test). Photo credit: Benhadou Farida, Laboratory of Stem Cells and Cancer.

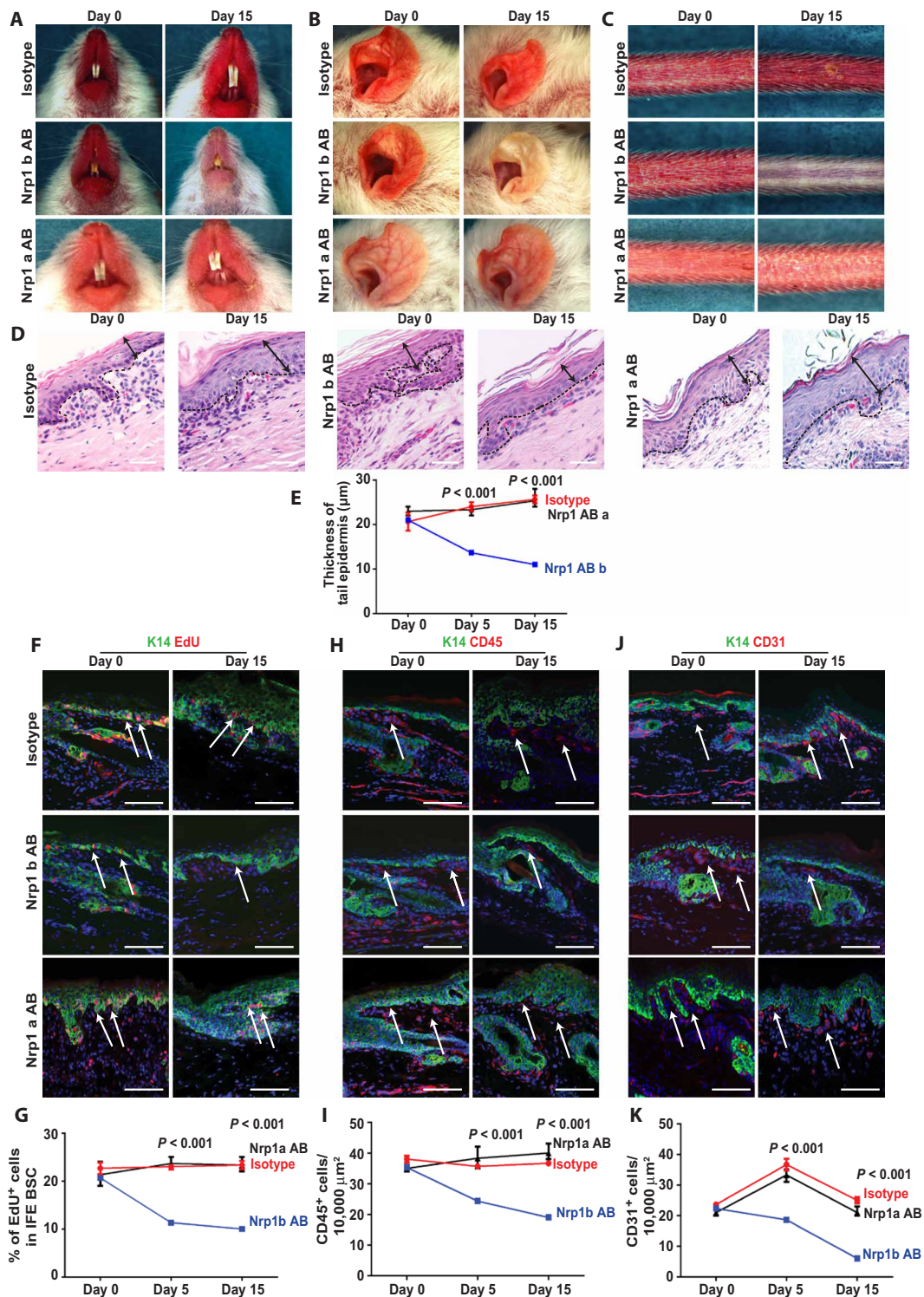


Fig. 3. Function-blocking anti-Nrp1 antibodies improve Vegfa-induced psoriasis. (A to C) Naso-oral region, ear, and tail, (D) H&E on tail skin. Scale bars, 50 µm. (E) Measures of epidermal thickness ($n = 3$) (means \pm SEM, Mann-Whitney). (F) K14/EdU staining. Scale bars, 50 µm. (G) Percentage of EdU-positive BCs [$n = 387$ (isotype, day 0), $n = 354$ (isotype, day 15), $n = 424$ (Nrp1b AB, day 0), $n = 409$ (Nrp1b AB, day 15), $n = 391$ (Nrp1a AB, day 0), $n = 421$ (Nrp1a AB, day 15) total BCs, $n = 3$] (means \pm SEM, Mann-Whitney). (H) K14/CD45 staining. Scale bars, 50 µm. (I) Density of CD45-positive cells in the dermal IFE area of 254,342 µm² (isotype, day 0), 298,567 µm² (isotype, day 15), 267,890 µm² (Nrp1b AB, day 0), 287,908 µm² (Nrp1b AB, day 15), 257,560 µm² (Nrp1a AB, day 0), 294,901 µm² (Nrp1a AB, day 15); $n = 10$. Number of CD45-positive cells per 10,000 µm² (means \pm SEM, Mann-Whitney). (J) K14/CD31 staining. Scale bar, 50 µm. (K) Microvascular density in dermal IFE area of 267,980 µm² (isotype, day 0), 234,589 µm² (isotype, day 15), 222,370 µm² (Nrp1b AB, day 0), 223,456 µm² (Nrp1b AB, day 15), 200,154 µm² (Nrp1a AB, day 0), and 212,980 µm² (Nrp1a AB at day 15). Number of CD31-positive cells per 10,000 µm² (means \pm SEM, Mann-Whitney). Photo credit: Benhadou Farida, Laboratory of Stem Cells and Cancer.

end, we induced the deletion of *Flt1* in the skin epidermis of *c-Jun/JunB* cKO mice, one of the most commonly used mouse model of psoriasis (16, 27). In this model, mice develop a strong psoriasis-like disease 2 weeks after *c-Jun/JunB* conditional deletion (fig. S4, A and B) (16).

Epidermal deletion of *Flt1* in this model (*c-Jun/JunB/Flt1 triple cKO*) decreased the severity of psoriasis lesions both macroscopically and microscopically with a decrease in epidermal thickness (fig. S4, C and D). The immune infiltrate within the epidermis, which consists mainly of neutrophils in this model, was normalized upon epidermal *Flt1* deletion (fig. S4, E to G). The microvascular density was also normalized upon *Flt1* deletion (fig. S4, G to I). These data demonstrate the conserved function of *Flt1* in epidermal cells to mediate psoriasis development across different psoriasis mouse models.

Transcriptional landscape associated with Vegf/Flt1/Nrp1 signaling in psoriasis

To define the molecular mechanisms that regulate the cell autonomous function of *Flt1* and *Nrp1* in epidermal cells to initiate psoriasis formation, we first defined the transcriptional signature of epidermal cells induced by *Vegfa* in the presence or absence of *Flt1* and *Nrp1*. To this end, we performed RNA sequencing on FACS-isolated basal keratinocytes from control, K14-*Vegfa*, K14-*Vegfa/Nrp1 cKO*, and K14-*Vegfa/Flt1 cKO* mice.

The majority of the genes up-regulated by *Vegfa* [382 of 968 genes (40%), $P = 10^{-17}$] were no longer up-regulated following either *Flt1* or *Nrp1* deletion, demonstrating that the core of the transcriptional changes that occur following *Vegfa* overexpression in epidermal cells is coregulated by *Flt1* and *Nrp1* (Fig. 4A). In contrast, 243 of the 968 genes up-regulated by *Vegfa* (25%, $P = 10^{-12}$) were up-regulated by *Vegfa* in all conditions irrespective of *Nrp1* and *Flt1* expression by keratinocytes, and thus, represent the genes that are regulated by *Vegfa* in keratinocytes independently of *Flt1/Nrp1* expression in epidermal cells (Fig. 4A). Last, 226 of 968 genes (23%, $P = 10^{-12}$) up-regulated by *Vegfa* were no longer up-regulated by *Vegfa* following *Flt1* deletion in K14-*Vegfa/Flt1 cKO* but were normally up-regulated following *Nrp1* deletion, and 117 of 968 genes (12%, $P = 10^{-11}$) were no longer up-regulated in the absence of *Nrp1* but normally regulated in the absence of *Flt1* (Fig. 4A). These data indicate that the vast majority of the genes up-regulated by *Vegfa* in the epidermis were dependent on *Flt1* and *Nrp1* expression by keratinocytes.

Gene ontology (GO) of the genes up-regulated by more than twofold by *Vegfa* overexpression and depending on *Flt1* and *Nrp1* expression by keratinocytes (382 of 968 genes) showed enrichment for transcripts regulating immunity ($P = 10^{-8}$), proliferation ($P = 10^{-8}$), and epidermal differentiation ($P = 10^{-6}$), as previously reported in human psoriasis and other murine models of psoriasis-like disease (Fig. 4B). We summarized the top up-regulated genes in table S1. Some of these genes were known to be involved in psoriasis, whereas many others have not been previously implicated in psoriasis but regulate cell functions potentially relevant for psoriasis development, such as the regulation of proliferation and epidermal differentiation.

In addition to the up-regulated genes, our analysis also showed that *Vegfa* overexpression also induced the down-regulation of 1225 genes by more than twofold. The majority of the down-regulated genes [602 of 1225 genes (49%), $P = 10^{-17}$] were dependent on the expression of both *Nrp1* and *Flt1* by keratinocytes, and an additional 227 of 1225 genes (19%, $P = 10^{-10}$) of the genes down-regulated by *Vegfa* were *Flt1* dependent but *Nrp1* independent (Fig. 4D). Only 8% ($P = 10^{-7}$) of the down-regulated genes were blocked by *Nrp1* deletion, but not

Flt1 deletion (Fig. 4D). In addition, 24% of these genes (296 of 1225, $P = 10^{-9}$) were down-regulated by *Vegfa* independently of the expression of either *Nrp1* or *Flt1* (Fig. 4D). GO of the genes down-regulated by more than twofold by *Vegfa* in an *Flt1*- and *Nrp1*-dependent manner (602 of 1225 genes) showed enrichment for transcripts inhibiting proliferation ($P = 10^{-21}$), regulating the extracellular matrix (ECM) ($P = 10^{-9}$) and epidermal differentiation ($P = 10^{-6}$) (Fig. 4E). We summarized the top down-regulated genes in table S2.

Together, our data demonstrated that most genes up-regulated and down-regulated by *Vegfa* overexpression in epidermal cells were dependent on the expression of both *Flt1* and *Nrp1* in keratinocytes, suggesting that the core of the transcriptional changes associated with psoriasis development induced by *Vegfa* is dependent on a cell autonomous function of *Flt1* and *Nrp1* in epidermal cells.

Chromatin remodeling associated with Vegfa/Flt1/Nrp1 signaling in psoriasis

To understand more globally the changes in the chromatin landscape that occur during *Vegfa*-mediated psoriasis-like disease and identify the transcription factors (TFs) and gene regulatory networks that control the changes in gene expression associated with psoriasis development, we FACS-isolated basal keratinocytes from control, K14-*Vegfa*, K14-*Vegfa/Nrp1 cKO*, and K14-*Vegfa/Flt1 cKO* mice and performed ATAC-seq, a technique that allows the mapping of the open chromatin regions with high definition and predicts the TFs that regulate chromatin remodeling (28). We first defined the chromatin remodeling associated with *Vegfa*-mediated psoriasis by assessing the chromatin regions (ATAC-seq peaks) that are changed by more than twofold between K14-*Vegfa* and control mice. We found that 16,863 chromatin regions were more open ($P = 10^{-11}$), and 5829 chromatin regions were more closed upon *Vegfa* overexpression ($P = 10^{-11}$). Among the peaks that were up-regulated upon *Vegfa* overexpression, we found that 9964 peaks (59%, $P = 10^{-15}$) were no more up-regulated upon *Flt1* or *Nrp1* deletion, 2703 peaks (16%, $P = 10^{-10}$) were no more up-regulated upon *Flt1* deletion only, 2366 peaks (14%, $P = 10^{-11}$) were no more up-regulated upon *Nrp1* deletion only, and 1830 peaks (11%, $P = 10^{-7}$) were unchanged following *Nrp1* or *Flt1* deletion (Fig. 5A).

Among the peaks that were down-regulated upon *Vegfa* overexpression, we found that 1723 peaks (30%, $P = 10^{-15}$) were no more down-regulated upon *Flt1* and *Nrp1* deletion, 1444 peaks (25%, $P = 10^{-13}$) were no more up-regulated upon *Flt1* deletion only, 595 peaks (10%, $P = 10^{-8}$) were no more up-regulated upon *Nrp1* deletion only, and 2067 peaks (35%, $P = 10^{-13}$) were unchanged upon *Nrp1* or *Flt1* deletion (Fig. 5B). We performed TF binding site motif analysis on the peaks that were up-regulated upon *Vegfa* overexpression in an *Flt1/Nrp1*-dependent manner. We found an enrichment in TF motifs corresponding to Gata TF (26%, $P = 10^{-185}$), TEAD TF (28%, $P = 10^{-41}$), Egr1 (14%, $P = 10^{-32}$), AP-1 (32%, $P = 10^{-26}$), basic helix-loop-helix (bHLH) TF (38%, $P = 1 \times 10^{-21}$), and Slug (14%, $P = 10^{-11}$) (Fig. 5C). Among the peaks that were down-regulated upon *Vegfa* overexpression in an *Flt1/Nrp1*-dependent manner, we found an enrichment in TF motifs corresponding to Klf TF (33%, $P = 10^{-19}$) and homeobox TF (30%, $P = 10^{-16}$) (Fig. 5D).

After assigning the genes associated with each of these peaks, we assessed which of these peaks up-regulated by *Vegfa* were associated with an increase in gene expression by more than twofold (peaks up/genes up) (Fig. 5E). We found that 937 genes fell into this category.

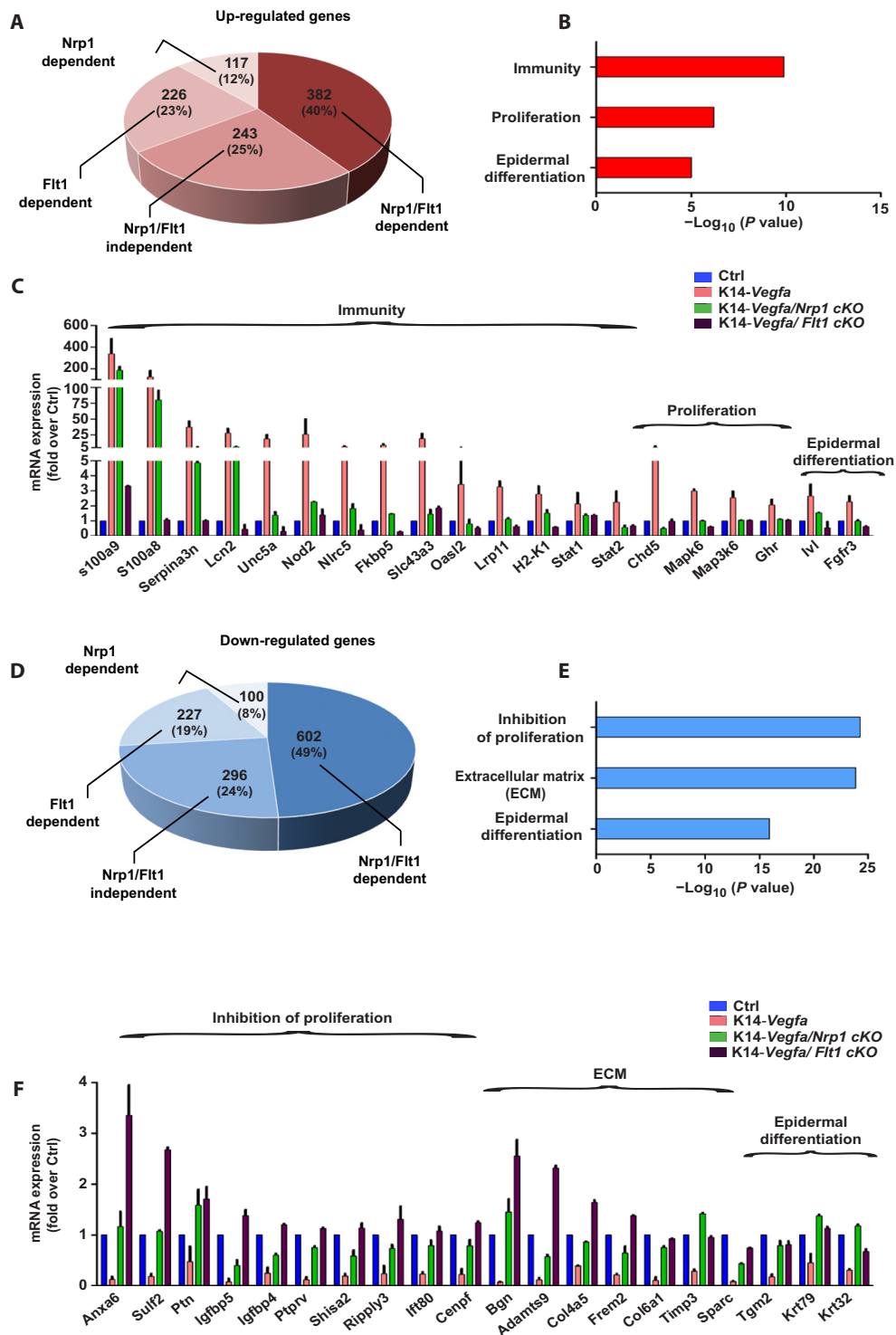


Fig. 4. Transcriptional landscape associated with Nrp1/Flt1/Vegfa signaling in psoriasis. (A) Pie chart showing the percentage of total up-regulated genes in K14-Vegfa and depending either on common Nrp1/Flt1 (=Nrp1/Flt1 dependent) or specifically on Nrp1 (=Nrp1 dependent) or Flt1 (Flt1 dependent) expression. Genes with unchanged expression after Nrp1 or Flt1 epidermal ablation were also represented (=Nrp1/Flt1-independent up genes). (B) GO analysis of up-regulated genes in Vegfa overexpression in an Nrp1- and Flt1-dependent manner. (C) mRNA relative expression of up-regulated genes by RNA-seq in Vegfa overexpression in FACS-isolated basal keratinocytes (n = 2) (means ± SEM). (D) Pie chart showing the percentage of total down-regulated genes in K14-Vegfa and depending either on common Nrp1/Flt1 expression (=Nrp1/Flt1 dependent) or specifically on Nrp1 (=Nrp1 dependent) or Flt1 (Flt1 dependent) expression. Genes with unchanged expression after Nrp1 or Flt1 epidermal ablation were also represented (=Nrp1/Flt1-independent down genes). (E) GO analysis of down-regulated genes in Vegfa overexpression in an Nrp1- and Flt1-dependent manner. (F) mRNA relative expression of down-regulated genes by RNA-seq in Vegfa-overexpressing mice and depending on Nrp1 or Flt1 expression in FACS-isolated keratinocytes (n = 2) (means ± SEM).

We then assessed which of these genes still present chromatin remodeling following Nrp1 or Flt1 deletion. The great majority of these genes (70%, 660 of 937, $P = 10^{-8}$) did not present significant change at these chromatin regions in the absence of Flt and Nrp1, and only 5% ($P = 10^{-5}$) of these genes (48/937) presented chromatin remodeling following *Vegfa* overexpression in the absence of Flt1 and Nrp1 (Fig. 5E), showing the key role of Flt1 and Nrp1 in epidermal cells to mediate the chromatin remodeling induced by *Vegfa* overexpression. GO analysis of the peaks up-regulated/genes up-regulated that are Nrp1/Flt1 dependent revealed that these genes were associated with the induction of initial phases of immune responses and type I interferon-induced genes ($P = 10^{-7}$) (Fig. 5F and table S3).

To get further insights into the gene regulatory network that controls psoriasis, we performed motif enrichment analysis of the chromatin regions that became more opened during *Vegfa*-mediated psoriasis development. Among the genes for which the ATAC-seq peaks in their regulatory regions were opened and accompanied by an increase in gene expression in an Flt1/Nrp1-dependent manner, we found that the most enriched TF motifs in these peaks were AP-1 TFs (32% of the peaks, $P = 10^{-23}$), NF1 (18% of the peaks, $P = 10^{-13}$), GATA TFs (34% of the peaks, $P = 10^{-11}$), P63 (18% of the peaks, $P = 10^{-11}$), CCCTC-binding factor (CTCF) (9% of the peaks, $P = 10^{-11}$), TEAD (35%, $P = 10^{-10}$), bHLH TFs (23%, $P = 10^{-10}$), consistent with the motifs found on all peak (Fig. 5G).

We then assessed which of the down-regulated peaks in K14-*Vegfa* epidermis were associated with down-regulation of gene expression by more than twofold (peaks down/genes down) (Fig. 5, H and I). Among these 467 genes, the vast majority of them were no longer down-regulated following *Flt1* or *Nrp1* cKO (60%, 279 of 467 for both cKO, $P = 10^{-8}$), 26% (123 of 467, $P = 10^{-7}$) following Flt1 deletion, and 4% ($P = 10^{-7}$) following Nrp1 deletion, whereas only 10% of these genes presented chromatin remodeling upon *Vegfa* expression independently of Nrp1 and Flt1 (43 of 490, $P = 10^{-6}$) (Fig. 5H).

Motif discovery analysis in the down-regulated peaks associated with down-regulation of gene expression in an Flt1/Nrp1-dependent manner revealed that Klf TFs (26% of the peaks, $P = 10^{-20}$), AP-1 TFs (33% of the peaks, $P = 10^{-14}$), and p63 (23% of the peaks, $P = 10 \times 10^{-13}$) were the most statistically significant TF motifs enriched in these down-regulated peaks (Fig. 5J).

Together, these data demonstrate that most of the chromatin remodeling associated with gene activation or repression induced by *Vegfa* is mediated by the cell autonomous function of Flt1 and Nrp1 in epidermal cells, and identify the TFs associated with the chromatin remodeling-mediated *Vegfa* in an Flt1- and Nrp1-dependent manner.

Fosl1 acts downstream of Vegfa/Flt1 signaling in promoting psoriasis

AP-1 binding sites were among the most significantly enriched TF motifs found in the chromatin regions of genes that were up-regulated in an Flt1- and Nrp1-dependent manner during *Vegfa*-induced psoriasis-like disease. AP-1 represents a family of TFs composed of Jun and Fos that function as homo- or heterodimer, and epidermal deletion of *c-Jun/JunB* leads to a psoriasis-like disease in mice (16).

Many of the chromatin regions of these *Vegfa*-regulated genes presenting AP-1 binding sites were no longer remodeled when Flt1 or Nrp1 was deleted from the epidermis (32%, 211 of 660 of the genes up-regulated; 33%, 92 of 279 of the genes down-regulated), consistent with a key role for Flt1/Nrp1 in regulating the chromatin remodeling associated with AP-1 TFs. GO analysis performed on

genes up-regulated/peaks up-regulated and containing AP-1 motifs showed enrichment in immunity-related genes (e.g., *Tlr4*, *Art3*, *Ikk2*, *Alox5ap*, and *Nlrp5*) (fig. S5A). GO analysis performed on genes down-regulated/peaks down-regulated and containing AP-1 motifs showed enrichment in ECM-related genes (e.g., *Tgfb2*, *Mmp13*, *Angiopl17*, *Ism1*, and *Tnfrsf19*) (fig. S5B).

These genes were similarly up-regulated or down-regulated by *Vegfa* signaling in in vitro-cultured keratinocytes and in the skin epidermis in vivo (fig. S5, C to F), further supporting the importance of a cell autonomous *Vegfa/Flt1/AP-1* signaling in keratinocytes that mediates psoriasis. We have confirmed the up-regulation of Toll-like receptor 4 (TLR4) and down-regulation of *Ism1* at the protein level by immunofluorescence on tail skin sections (fig. S5G). To determine which AP-1 TFs relay *Vegfa* signaling to induce the chromatin remodeling and change in gene expression associated with psoriasis, we assessed which members of the AP-1 family are up- or down-regulated following *Vegfa* overexpression. We found that among AP-1 TFs, only Fosl1 was up-regulated by *Vegfa* overexpression (Fig. 6A). Fosl1 overexpression was no longer up-regulated following *Flt1* deletion in K14-*Vegfa/Flt1* cKO mice, showing the importance of cell autonomous *Vegfa/Flt1* signaling in promoting Fosl1 overexpression. In addition, we also demonstrated the overexpression of Fosl1 in epidermal cells by immunohistochemistry on skin section in the K14-*Vegfa* and *c-Jun/JunB* cKO psoriasis models (fig. S6, B and C).

To directly and functionally assess the importance of Fosl1 in the cell autonomous *Vegfa/Flt1* signaling that promotes psoriasis development, we performed short hairpin RNA (shRNA) knockdown of Fosl1 in mouse cultured keratinocytes in vitro and assessed the impact of Fosl1 down-regulation on chromatin remodeling and change in gene expression mediated by *Vegfa* signaling. Primary culture of keratinocytes from epidermis was infected with lentiviruses expressing shRNA against Fosl1, stimulated or not with *Vegfa* (50 ng/ml) (Fig. 6, D to F) and then assessed for change in gene expression and chromatin accessibility using real-time ATAC-PCR and qRT-PCR (Fig. 6, G to J). It is important to note that the addition of *Vegfa* to primary cultured keratinocytes is important, as the level of *Vegfa* by the *Rosa* promoter may not be strong enough to promote angiogenesis in the absence of secretion of other angiocrine factors by the keratinocytes in response to autocrine *Vegfa* signaling in those cells. In addition, *Vegfa* induced the phosphorylation of Flt1 in 293T cells transfected with Flt1-Flag expression plasmids and in keratinocytes in vitro (fig. S6, A to C), similarly to what has been reported in tumor cells (15, 29). Western blot analysis showed that Fosl1 shRNA down-regulated Fosl1 efficiently (Fig. 6, D and F). ATAC-PCR showed that Fosl1 knockdown blocked the chromatin remodeling associated with *Vegfa/Flt1/AP-1* signaling in keratinocytes in vitro (Fig. 6, G and H), resulting in the absence of up- or down-regulation of these genes upon *Vegfa* signaling in vitro (Fig. 6, I and J). Together these results demonstrate the key role of Fosl1 in mediating chromatin remodeling and changes in gene expression associated with *Vegfa/Flt1/AP-1* signaling during psoriasis development.

DISCUSSION

Our study uncovers the essential epidermal autonomous functions of Flt1 and Nrp1 in promoting *Vegfa*-induced psoriasis-like disease (fig. S7). Several case studies have previously reported the improvement of psoriatic disease in patients with cancer treated with anti-VEGFA

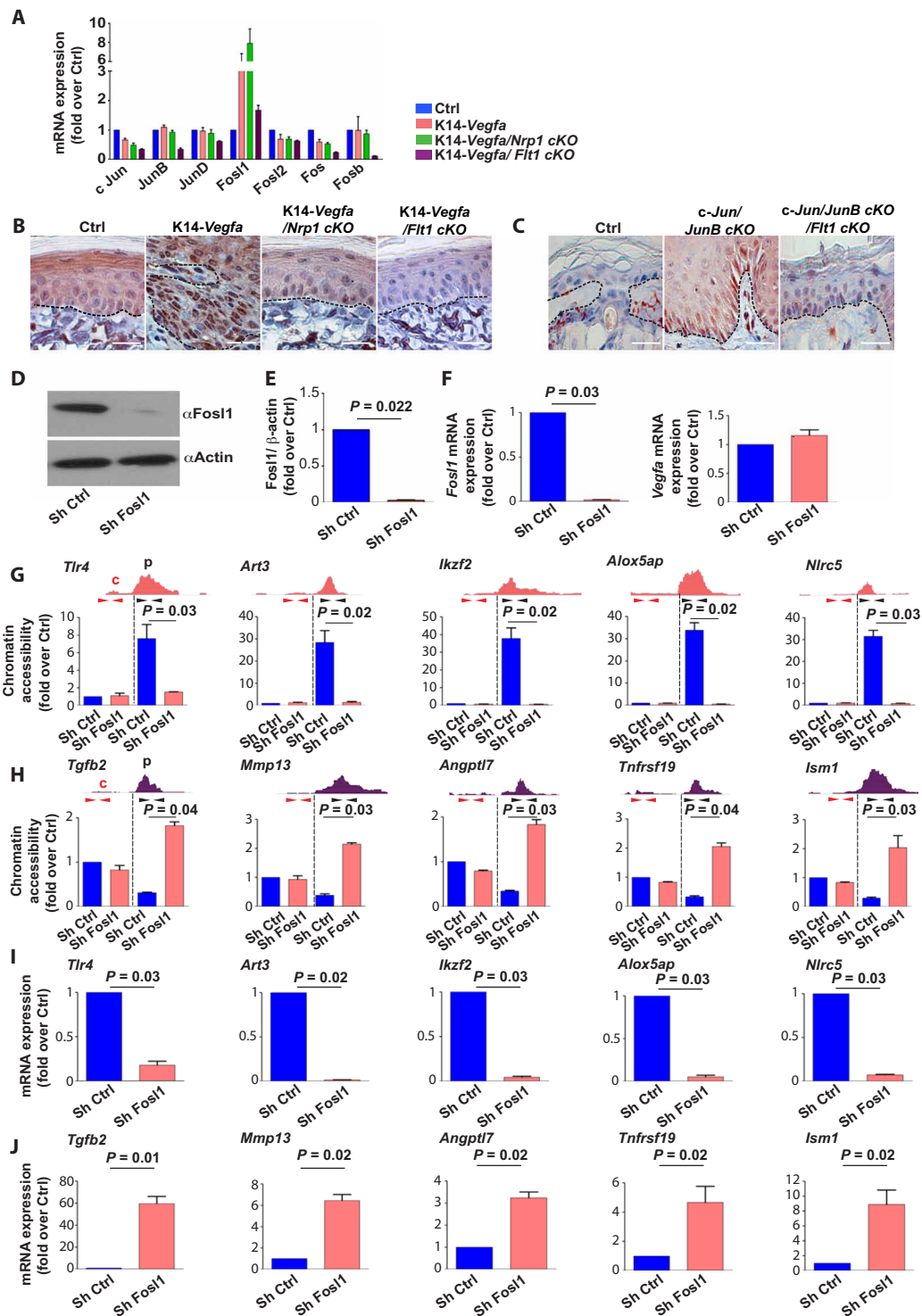


Fig. 6. Fosl1 acts downstream of Vegfa/Flt1 signaling in the regulation of chromatin remodeling and transcriptional change associated with psoriasis. (A) mRNA expression of AP-1 members by RNA-seq in FACS-isolated basal keratinocytes ($n=2$) (means \pm SEM). (B) IHC (immunohistochemistry) of Fosl1 nuclear staining in tail epidermis. Scale bars, 10 μ m. (C) IHC of Fosl1 in ear epidermis. Scale bars, 10 μ m. (D) Fosl1 expression assessed by Western blot on primary cultured keratinocytes from K14-Vegfa after transduction with control (sh Ctrl) or Fosl1-specific shRNA (sh Fosl1). (E) Protein expression of Fosl1 ($n=3$). Histogram represents means \pm SEM. (F) Vegfa and Fosl1 mRNA expression measured par qRT-PCR on primary cultured keratinocytes from K14-Vegfa transduced with sh Ctrl or sh Fosl1 ($n=3$) (means \pm SEM, Mann-Whitney). (G) Relative chromatin accessibility measured by ATAC qPCR of chromatin regions presenting AP-1 binding sites in the regulatory regions of up- or down-regulated genes (H) in primary cultured keratinocytes from K14-Vegfa transduced with sh Ctrl or sh Fosl1 ($n=3$). Primers were designed around the control region (c) and peak region (p) (means \pm SEM, Mann-Whitney). (I) mRNA expression by qRT-PCR of up- or down-regulated genes (J) presenting AP-1 binding sites in their regulatory regions in primary cultured keratinocytes from K14-Vegfa transduced with sh Ctrl or sh Fosl1 ($n=3$) (means \pm SEM, Mann-Whitney test).

antibodies or anti-VEGFA receptor small-molecule inhibitors (30, 31). Likewise, the use of anti-VEGFA inhibitors in different mouse models of psoriasis (K14-*Vegfa*, epidermal deletion of *c-Jun/JunB*) induced regression of the psoriasis phenotypes including epidermal hyperproliferation, thickness, altered differentiation, dermal immune infiltration, and increased angiogenesis (7, 8, 32, 33). In these studies, it was thought that anti-VEGFA therapy acts by targeting ECs and immune cells located in the dermis. In sharp contrast, our study shows that most of the psoriasis phenotypes mediated by *Vegfa* on keratinocytes, immune cells, and ECs are the consequences of *Vegfa* signaling in keratinocytes in an *Flt1/Nrp1*-dependent manner. The cell autonomous role of *Flt1* and *Nrp1* in *Vegfa*-induced psoriasis is reminiscent of the autocrine or paracrine role of *Vegfa* in promoting skin tumor progression and cancer stem cell function (14, 15).

The decrease in neoangiogenesis and immune cell infiltration in the absence of *Nrp1* and *Flt1* expression in the epidermis suggests that the keratinocytes are essential to orchestrate the vascular remodeling and immune cell infiltration. RNA-seq showed that upon *Vegfa* signaling, keratinocytes expressed chemoattractants for immune cells (e.g., *S100A8/A9*) and proangiogenic molecules (e.g., *Adm*), which together with *Vegfa* regulate the neoangiogenesis and immune infiltration associated with the psoriasis phenotype.

By performing RNA-seq and ATAC-seq of FACS-isolated basal keratinocytes in the presence of *Vegfa* overexpression and in the presence or absence of *Nrp1* or *Flt1* expression, we defined the changes in the chromatin and transcriptional landscape associated with the cell autonomous signaling of *Vegfa* in mediating psoriatic-like disease. Our bioinformatics analysis of these molecular changes uncovers *Fos1* in regulating gene expression mediated by *Vegfa/Flt1* signaling in keratinocytes. Moreover, the *Vegfa/Flt1/Nrp1* keratinocyte cell autonomous epigenetic and transcriptional signatures uncovered here may represent novel biomarkers to predict the response of antipsoriatic treatments. The rapid improvement of psoriatic-like disease following the administration of anti-*Nrp1* blocking antibodies that specifically target the interaction between *Nrp1* and *Vegfa* demonstrates the therapeutic potential of blocking the *Nrp1/Vegfa* interaction in psoriasis.

In conclusion, our study demonstrates a keratinocyte autonomous function of *Nrp1* and *Flt1* in mediating *Vegfa* signaling in the epidermis and the development of psoriatic-like disease in mice. These results have important implications for our understanding of the pathogenesis of psoriasis and open new avenues for psoriasis treatment.

MATERIAL AND METHODS

Study design

The study was conducted on mouse models as described in the “Experimental models” section to perform in vivo and in vitro laboratory experiments. The sample size was not predetermined. We used a sample size allowing statistical significance to be reached between the different groups. No animals were excluded from the analysis. No technical replicates were used to calculate statistics. No randomization and no blinding were used in this study. For each experiment, we used biological-independent replicates per condition, and the number of replicate has been reported in the legends.

Experimental models

K14-Cre (34) mice were mated with *Rosa26-VEGF-164* (35), *Nrp1^{fl/fl}* (36), and *Flt1^{fl/fl}* (37) mice. All mice used in this study were com-

posed of males and females with mixed genetic background. Mouse colonies were maintained in a certified animal facility in accordance with the European guidelines and with approved ethical protocol (no. 526N).

Primary cell culture

Tail skin was removed from the tail bone and incubated overnight at 4°C in Hanks’ balanced salt solution (HBSS) (Gibco) and 0.25% trypsin (Gibco). The epidermis was then separated from the dermis and incubated on a rocking plate (100 rpm) at room temperature for 5 min. Basal cells were mechanically separated from the epidermis by flushing 10 times under the epidermis. Trypsin was then neutralized by adding Dulbecco’s modified Eagle’s medium. (DMEM) (Gibco) supplemented with 5% Chelex fetal calf serum (FCS) and filtrated on a 70- μ m filter (Falcon). Cells were cultured in MEM supplemented with 10% FBS, hydrocortisone (0.4 μ g/ml), epidermal growth factor (10 ng/ml), 2×10^{-9} MT3, 1% penicillin/streptomycin, 2 mM L-glutamine and incubated at 37°C with 20% O₂ and 5% CO₂. Twenty-four hours later, the cells were treated with recombinant vascular endothelial growth factor (VEGF) (50 ng/ml; R&D).

Virus production, infection, and selection

Stable knockdown cell lines were generated using lentiviral pLKO/PuroR vectors (Sigma-Aldrich) after puromycin selection (2.5 μ g/ml). Knockdown was confirmed by qRT-PCR and Western blot. Three different shRNAs (NM_010235.1-664s1c1, NM_010235.1-1050s1c1, and NM_010235.1-851s1c1) were used to target the same gene.

For virus production, 5×10^6 human embryonic kidney (HEK) 293T cells were seeded into 10-cm dishes and transfected with the vector of interest and appropriate packaging plasmids psPax2 and pMD2.G (12260 and 12259, respectively; Addgene). Medium was changed 24 hours later, and supernatants were collected at 48 hours and passed through a 0.45- μ m filter. Keratinocytes were plated in six-well plate cells and incubated with viruses (40 μ l/ml) when they reach 50% of confluence in the presence of polybrene (5 μ g/ml). Medium was changed 24 hours later, and infected cells were selected by puromycin (5 μ g/ml) for at least 1 week.

Antibodies

The following primary antibodies were used: anti-Ki67 (rabbit, 1:200, Abcam, catalog number ab15580), anti-K14 (rabbit, 1:1.000, Thermo Fisher Scientific, catalog number PA5-28002), anti-*Nrp1* (goat, 1:100, R&D, catalog number AF 566), anti-CD31 (rat, 1:200, BD Biosciences, Clone MEC13.3, catalog number 550274), anti-CD45 (rat, 1:500, BD Biosciences, clone 30F11, catalog number 12-0451/553081), anti-*Fos1* (mouse, 1:500, Santa Cruz, clone C12, catalog number sc-28310), CD4 (rat, 1:100, BD Biosciences, clone RM4-5, catalog number 565650), CD8 (rabbit, 1:100, Abcam, catalog number ab203035), CD19 (rat, 1:100, BD Biosciences, clone 1D3, catalog number 561737), Ly6G (rat, 1:100, BioLegend, clone 1A8, catalog number 177603), F4/80 (rat, 1:500, Serotec, clone A3-1, catalog number MCA497 GA), TLR4 (rabbit, 1:100, Abcam, ab22048), and ISM1 (rabbit, 1:100, Abcam ab103338). The following secondary antibodies were used: anti-rabbit, anti-rat, and anti-chicken conjugated to Alexa Fluor 488 (1:400, Molecular Probes), to Rhodamine Red-X, or to Cy5 (1:400, Jackson ImmunoResearch).

Western blot analysis

Keratinocytes were lysed in radioimmunoprecipitation assay (RIPA) buffer for 4 hours on ice and then centrifuged for 10 min at 14.000 rpm

at 4°C. Forty micrograms of cell lysate was loaded in 4/12% bis/tris-acrylamide gel (Invitrogen) and separated by electrophoresis. Proteins were transferred on polyvinylidene difluoride (PVDF) membranes. The membranes were incubated overnight with anti-Nrp1 (goat, 1:200, R&D, catalog number AF 566) or anti-Flt1 (mouse, 1:1000, Santa Cruz, clone H-225, catalog number sc-9029) or anti-Fos1 (mouse, 1:1000, Santa Cruz, clone C12, catalog number sc-28310) or Flt1 (rabbit, 1:1000, Abcam, ab3252) or anti-phospho-Flt1 Y1213 (rabbit, 1:1000, R&D, catalog number AF4170), (mouse, 1:1.000, Cell Signaling, catalog number 9106), anti-HA (human influenza hemagglutinin tag) (mouse, 1:1000, Sigma-Aldrich, catalog number: 11583816001), and anti- β -actin (1:3000, Abcam, catalog number ab8227). Anti-mouse or anti-rabbit immunoglobulin G (IgG) conjugated with horseradish peroxidase (HRP) (1:3000 or 1:10,000; Healthcare) was used as the secondary antibody.

Immunoprecipitation assay

hFlt1-HEK293 lysates were immunoprecipitated by incubation with anti-HA (1 μ g of antibody per 1.5 mg of protein, rabbit, Abcam, ab9110) coupled to Protein G Dynabeads (Invitrogen, catalog number 10003D) overnight at 4°C. Proteins were eluted in sample buffer by heating to 70°C for 10 min. For Western blot analysis, equal amounts of total protein were loaded and resolved on a NuPAGE 4/12% bis/tris gel (Invitrogen) and transferred to a PVDF membrane. Blots were probed with specific antibodies for HA-tag (mouse, 1:1000, Sigma, catalog number 11583816001), Flt1 (rabbit, 1:1000, Abcam, ab3252), and anti-PFlt1 (rabbit, 1:1.000, R&D, Y1213). Enhanced chemiluminescence anti-mouse or anti-rabbit IgG conjugated with HRP (1:3000 or 1:10,000; Healthcare) was used as the secondary antibody.

Phosphorylation assay for Flt1

Cells were serum starved for 12 hours and stimulated either by rVEGFA (50 ng/ml; R&D, catalog number 293 CF) or by hPLGF (human placental growth factor) (50 ng/ml; R&D, catalog number 264-PGB). We used as control condition nonstimulated transfected hFlt1-HEK293 cells as previously described (13).

Nrp1 antibody treatment

Mice were treated by Nrp1-blocking antibodies: anti-Nrp1a, which blocks binding of semaphorins, and anti-Nrp1b, which blocks binding of Vegfa (Genentech, 10 mg/kg) by intraperitoneal injection, two times per week during 15 days as described previously for tumor models (14, 26). The antibodies were generated and provided by Genentech.

Histology and immunostaining

Skin was embedded in OCT (optimal cutting temperature) (Tissue-Tek). Samples were sectioned at 4- to 6- μ m sections using CM3050S cryostat (Leica Microsystems GmbH). For the staining on frozen sections, tissues were fixed in 4% paraformaldehyde for 10 min at room temperature, and then washed in phosphate-buffered saline (PBS). Non-specific antibody binding was blocked with 5% horse serum, 1% bovine serum albumin, and 0.2% Triton X-100 during 1 hour at room temperature. Primary antibodies were incubated overnight at 4°C in blocking buffer. Sections were rinsed in PBS and incubated with secondary antibodies during 1 hour at room temperature. Nuclei were stained with Hoechst (4 mM). Slides were mounted using Glycergel (Dako) supplemented with 2.5% DABCO (Sigma-Aldrich). For the staining on paraffin sections, 4- μ m paraffin sections were deparaffinized and

rehydrated. Antigen unmasking was performed in citrate buffer (pH 6) at 98°C for 20 min using the PT (pre-treatment) module. Endogenous peroxidase was blocked using 3% H₂O₂ (Merck) in methanol for 20 min at room temperature. Endogenous avidin and biotin were blocked using the Endogenous Blocking kit (Invitrogen) for 20 min at room temperature. Primary antibodies were incubated overnight at 4°C. Anti-mouse biotinylated secondary antibodies, as well as Standard ABC kit, and ImmPACT DAB (Vector Laboratories) were used for the detection of HRP activity. Slides were mounted using SafeMount (Labonord).

Image acquisition

Microscopic imaging was performed on a Zeiss Axio Imager M1 (Thornwood) fluorescence microscope with a Zeiss AxioCam MR3 camera and a Zeiss AxioCam MRC5 camera for bright-field microscopy using the Axiovision release 4.6 software. Brightness, contrast, and picture size were adjusted using Photoshop CS6 (Adobe). Macroscopic imaging were performed using a Leica DFC 420C camera with an objective Leica 10446261 0.63 \times .

FACS isolation of epithelial cells for RNA sequencing

Tail skin was removed from the tail bone and incubated overnight at 4°C in HBSS (Gibco) and 0.25% trypsin (Gibco). The epidermis was then separated from the dermis and incubated on a rocking plate (100 rpm) at room temperature for 5 min. Basal cells were mechanically separated from the epidermis by flushing 10 times under the epidermis. Tissues were then cut into small pieces with a scalpel and incubated again for 5 min on a rocking plate (100 rpm) at room temperature. Trypsin was then neutralized by adding DMEM (Gibco) supplemented with 5% Chelex-treated FCS, and the cells were mechanically separated by pipetting 10 times and filtrated on a 70- μ m filter (Falcon). Cells were incubated in 2% FCS/PBS with primary antibodies for 30 min on ice. Cells were washed with 10 ml of 2% FCS/PBS and then incubated for 30 min in APC (allophycocyanin)-conjugated streptavidin (BD Biosciences), and then washed again and resuspended in 200 μ l of 2% FCS/PBS with Hoechst (10 mg/ml) diluted at 1:4000. Living epidermal cells were gated by forward scatter, side scatter, and negative for Hoechst. Basal interfollicular epidermis keratinocytes were stained using fluorescein isothiocyanate-conjugated anti- α_6 integrin (clone GoH3, 1:200, eBioscience, catalog number MAB1378) and biotinylated CD34 (clone RAM34, 1:50, BD Biosciences, catalog number 13-0341), followed by avidin/APC-streptavidin used to stain and exclude hair follicle stem cells. Basal keratinocytes were isolated on the basis of α_6 integrin expression with exclusion of CD34-positive cells. In Vegfa overexpression conditions, basal keratinocytes expressing the transgene are GFP positive, and we labeled basal keratinocytes using PE-conjugated anti- α_6 integrin (clone GoH3, 1:200, eBioscience, catalog number MAB1378), and bulge cells were labeled with biotinylated CD34 (clone RAM34, 1:50, BD Biosciences). We used PE-conjugated anti-CD45 (clone 30-f11, 1:200, eBioscience, catalog number 12-0451/553081), PE-conjugated anti-CD31 (clone MEC13.3; 1:100, BD PharMingen, catalog number 550274), and PE-conjugated anti-Pdgfra (clone APA-5, 1:200 eBioscience, catalog number 12-1401/624049) to exclude dermal cells and avoid dermal contamination, and anti-mouse/human CD11b (clone M1/70, BioLegend), anti-mouse CD16/32 (clone 93, BioLegend), anti-mouse Ly6C (HK1.4, BioLegend), and anti-mouse Ly6G (1A8, BioLegend) were used to gate for neutrophils, macrophages, and monocytes. FACS analysis was performed using FACS Aria I at high pressure (70 psi) and FACSDiva software (BD Biosciences). Sorted cells were collected into lysis buffer for RNA extraction.

RNA extraction and real-time RT-PCR

RNA extraction from FACS-isolated cells was performed using the RNAeasy Micro Kit (QIAGEN) according to the manufacturer's recommendations with DNase (deoxyribonuclease) treatment. After NanoDrop RNA quantification, the first-strand cDNA was synthesized using Superscript II (Invitrogen) and random hexamer (Roche) in 50 μ l of final volume. Control of genomic contamination was measured for each sample by performing the same procedure with or without reverse transcriptase. qPCR assays were performed using 1 ng of cDNA as template, SYBR Green Mix (Applied Bioscience) and a LightCycler 96 (Roche) real-time PCR system. β -Actin housekeeping gene was used for normalization. Primers were designed using the Roche Universal Probe library assay design center: <https://lifescience.roche.com/webapp/wcs/stores/servlet/CategoryDisplay?tab=Assay+Design+Center&identifier=Universal+Probe+Library&langId=-1>. qPCR analysis was performed using LightCycler 96 (Roche) real-time PCR system and the DDCT (Delta Delta CT) method with β -actin as a reference.

List of primers

Primers used for RT-qPCR are listed in Table 1.

ATAC-seq and library preparation

ATAC followed by sequencing was performed as follows: 100,000 sorted cells were collected in 1 ml of PBS and 3% FBS at 4°C. Cells were centrifuged, and then cell pellets were resuspended in 100 μ l of lysis buffer (10 mM tris-HCl, 10 mM NaCl, 3 mM MgCl₂, and IGEPAL 0.1%) and centrifuged (500g) for 25 min at 4°C. Supernatant was discarded, and nuclei were resuspended in 50 μ l of reaction buffer (2.5 μ l of Tn5 transposase, 22.5 μ l of tagmentation DNA buffer, and 25 μ l of H₂O-Nextera DNA Sample Preparation Kit, Illumina). The reaction was performed for 30 min at 37°C and then blocked by the addition of 5 μ l of clean-up buffer (900 mM NaCl and 300 mM EDTA). DNA was purified using the minElute purifi-

cation kit (QIAGEN) following the manufacturer's protocol. DNA libraries were PCR amplified (Nextera DNA Sample Preparation Kit, Illumina) and size selected from 200 to 800 base pairs (bp) (BluePippin, Sage Sciences) following the manufacturer's recommendations.

Samples for the ATAC qPCR experiment were processed in the same manner, and primers were designed around the control region and peak region. Primers are listed in Table 2.

ATAC-seq analysis

Two samples of control, K14-*Vegfa* and K14-*Vegfa/Nrp1 cKO*, and one sample of K14-*Vegfa/Flt1 cKO* were sequenced. ATAC-seq paired-end reads of 50 bp were trimmed for adaptor sequences using Trimmomatic. ATAC-seq paired-end reads were then aligned to the mouse GRCh38 genome using Bowtie2 (version 2.2.6) using options “-X 2000 --fr --very-sensitive --no-discordant --no-unal --no-mixed --non-deterministic.” More than 18 million reads were mapped to mouse genomic DNA in each condition (between 18 and 86 millions). Mitochondrial reads and reads aligned to scaffolds and undefined chromosomes were excluded from downstream analysis.

Reads with a mapping quality lower than 20 were eliminated with samtools, and duplicated reads were removed by Picard tools (<http://broadinstitute.github.io/picard/>). Read start sites were adjusted to represent the center of the transposon binding event as described in (38). Peak calling was performed on each individual sample using Macs2 (version 2.1.0.20151222) with parameter setting of “callpeak -f BAMPE -g mm -q 0.05 --nomodel --call-summits -B -SPMR.” Peaks from all ATAC-seq samples were merged for downstream analysis using bedtools. Pileup bedgraph files generated by MACS2 were transformed to tdf files with Integrative Genomics Viewer (IGV) tools, allowing the visualization of alignment data tracks by IGV. Read counts of each merged peaks for each individual sample were calculated by HTSeq-count using options “-s no -m intersection-nonempty.” These counts were normalized for 1 million of mapped reads in merged peaks, and fold of change was computed for all

Table 1. List of qPCR primers for mouse.

Gene name	Forward (5'-3')	Reverse (5'-3')
<i>Nrp1</i>	CATCTCCCGTTACCCCTATTCTT	GCGGCCGCCTTCATTCTC
<i>Vegfa</i>	TGGGCTCTTCGCTCCGCTAGTAG	GCCGCCTCACCCGTCAT
<i>Fos1</i>	CAAGTGGTTCAGCCCAAGAA	CACAAGGTGGAACCTCTGCTG
<i>Flt1</i>	AAAGGCTGAGCATCACTCCC	CTACAGGTGTAGAGGCCCGT
<i>Flk1</i>	TGTGCTTCTGTCTCTGGCG	CCTTCAAAGCCTTGACCTCG
<i>Art3</i>	CTGGGAGCGCAGTCTAATGG	CAGGTATTCTGCTCAAACGC
<i>Nlrc5</i>	AACCAATGTCTGTGCCCTGT	CTGGCTGCTCAGAAGTGGTA
<i>Alox5ap</i>	CTCATTTTGCGGTCGCTATCC	ATCCATGCCATTGTAGCCGTA
<i>Ikzf2</i>	GAGCCGTGAGGATGAGATCAG	CTCCCTCGCCTTGAAGGTC
<i>Tlr4</i>	TCGACATGGATCAGTTTATGCG	CCCTGGTACTGTTGTAGATGGA
<i>Ism1</i>	AGAGCAGCCAGATATGATTCC	GCCGCTGCTCTGAAAGTATCT
<i>Mmp13</i>	CTTCTTCTTGTGAGCTGGACTC	CTGTGGAGGTCACTGTAGACT
<i>Angptl7</i>	AGAGGCCCCAGCTTATCCAA	CAGGGGTATAGCTTCAAGGC
<i>Tgfb2</i>	TCGACATGGATCAGTTTATGCG	CCCTGGTACTGTTGTAGATGGA
<i>Tnfrsf19</i>	TTCTGTGGGGACACGATG	AGAAAATTACGCGCAGATGGAA
<i>B actin</i>	CCAGCCTTCTTCTGGGTAT	TGTTGGCATAGAGGTCTTACGG

Table 2. List of ATAC qPCR primers.

Control region		
Gene name	Forward (5'-3')	Reverse (5'-3')
<i>Nlrc5</i>	AAGGAACGGAGACAGAAGCG	AAAGGAGCAAGACCACCTCG
<i>Alox5ap</i>	GTACAGGGGCAGGTGTTTCA	AAGTCTTCCTTGCCCTGG
<i>Ikzf2</i>	CCTCAGCTTCCACACTCTG	CTCCTCCTGCATCAGTCTTGA
<i>Tlr4</i>	TTCTTGGGAAACACTTGGTGAAT	GCTGAGAGGAAGATTGCTT
<i>Ism1</i>	GTACAACGCTGGGAGATTCC	ATCTGAGCCCAACCTGGATGA
<i>Mmp13</i>	AAGCTGGCTCAGTCTGTTTT	GTAGGGGCAGAGGAAGGGA
<i>Angptl7</i>	AGGAGGCTAGTCCGATAGGG	AAACCGCAGTACCAGTGCAA
<i>Tgfb2</i>	GCAACTGCCATTTCTGGGC	GGATGGGACAGCCATCTT
<i>Tnfrsf19</i>	CCAATCTCAGGGCAGGGTT	AGAACTGTTCCAACCCACT
Peak region		
<i>Art3</i>	TCCCAGGGAACCTCAAAGG	GCTTTCACCTCCAGTGGCT
<i>Nlrc5</i>	GGTTGGGGTGGGGGTAT	ATGTGAATTACTAAGGACATGGG
<i>Alox5ap</i>	TAGACTCAGGCCAAACCCCT	GCCAGTGTCTATCAAGCCT
<i>Ikzf2</i>	TTCTGACTAGCCCATCCA	CAGGACCTGGGTTTTAGCCT
<i>Tlr4</i>	ACTCAGACTGATCCTGCTTG	AATGTGAGCCTTCTCCCAA
<i>Ism1</i>	TTCTGGGTGTGGGTGGTCTA	GGAACTGAAGCCTTCTGCC
<i>Mmp13</i>	GAGGAGGCATGGGTATGGTC	AGAAAGCAGTTGGTTGGCCC
<i>Angptl7</i>	GGGAGCCTCAATTCTCTCTG	CCATTGATGGGATTGTGTTTTGT
<i>Tgfb2</i>	AGAGTATGGCTGGCTCTCCA	TGGGTACAATGAGATGGGC
<i>Tnfrsf19</i>	AAACGAATGTGCTGCACGA	TGTGCGACAGATTGACCCCTG

Table 3. Statistical analysis performed for each experiment.

Figures	Normal distribution		Equality of variances		Comparison tests	
	Yes	No	Yes	No	Student's t test	Mann-Whitney
1 (B and D)		✓				✓
1 (G, I, K, and M)	✓		✓		✓	
2 (B and D)		✓				✓
2 (G, I, K, and M)	✓		✓		✓	
3 (E, I, J, and K)		✓				✓
6 (F to K)		✓				✓
S1 (D, F, H, and J)	✓		✓		✓	
S1K		✓				✓
S2B		✓				✓
S2D		✓				✓
S3 (F to H)		✓				✓
S4 (D to F and I)	✓		✓		✓	
S5 (C to F)		✓				✓
S6C		✓				✓

pairwise comparisons on the means of read counts (for control, K14-*Vegfa*, and K14-*Vegfa/Nrp1 cKO*) or on the read count (for K14-*Vegfa/Flt1 cKO*). Peaks up-regulated were defined as those having at least a twofold change, and merged peaks nonintersecting a peak called with

a *q* value of 0.05 in the up-regulated condition were removed. Peaks were associated to genes with the GREAT software with the following association rules: “basal plus extension” with parameters 5.0 kb in proximal upstream, 1.0 kb in proximal downstream, and 100.0 kb in distal.

Motif analysis

De novo motif search was performed using the findMotifsGenome.pl program in the HOMER package with parameter setting of “-size -250,250 -S 15 -len 6,8,10,12,16.” Incidences of specific motif were examined by the program of annotatePeaks.pl in the HOMER package with default parameters.

GO analysis

Genes up- or down-regulated between were tested for enrichment in each GO class using the DAVID web server. Statistically significant enrichments correspond to those presenting a Benjamini-corrected *P* value less than or equal to 0.05.

Quantification and statistical analysis

All the statistical analyses were based on biological replicates (*n* is indicated in the text, figures, or figure legends). The statistical tests used for each experiment have been added to the corresponding figure legends. Statistical analysis was performed using GraphPad Prism version 7.00 for Windows (GraphPad Software). Before performing the statistical analysis, we checked the distribution of the data by performing the Shapiro-Wilkinson test, and we checked the equality of variances between two comparisons by performing the Fisher-Snedecor test. Comparisons between two groups were carried out using an unpaired two-tailed Student's *t* test if the data were normally distributed and if the variances were equal between the two comparisons. Comparisons between two groups were carried out using the Welsh test if the data were normally distributed and if the variances were not equal between the two comparisons. If the data were not normally distributed, Mann-Whitney test was performed. Data are presented as the arithmetic means \pm SEM. The normality of the distribution of the data and the equality of the variances between the groups were verified. Based on this, the means of the groups were compared using the most appropriate comparison tests as summarized in Table 3.

SUPPLEMENTARY MATERIALS

Supplementary material for this article is available at <http://advances.sciencemag.org/cgi/content/full/6/2/eaax5849/DC1>

Fig. S1. Vegfa overexpression in the epidermis mediates psoriasis-like disease.

Fig. S2. Composition of immune infiltrate.

Fig. S3. Nrp1 and Flt1 are genetically linked.

Fig. S4. Epidermal autonomous expression of Flt1 is essential for psoriasis development induced by *c-Jun/JunB* deletion.

Fig. S5. Genes presenting AP-1 motifs in the chromatin regions remodeled by Vegfa/Flt1 signaling.

Fig. S6. Phosphorylation assay.

Fig. S7. Model of the epidermal autonomous VEGF/Flt1/Nrp1 signaling in psoriasis-like disease.

Table S1. Biological functions of up-regulated genes in an Nrp1/Flt1-dependent manner.

Table S2. Biological function of down-regulated genes in an Nrp1/Flt1-dependent manner.

Table S3. Biological function of genes associated with ATAC peaks in an Nrp1/Flt1-dependent manner.

[View/request a protocol for this paper from Bio-protocol.](#)

REFERENCES AND NOTES

- R. G. Langley, G. G. Krueger, C. E. Griffiths, Psoriasis: Epidemiology, clinical features, and quality of life. *Ann Rheum Dis* **64** Suppl. 2, ii18–ii23 (2005).
- M. A. Lowes, M. Suarez-Farinas, J. G. Krueger, Immunology of psoriasis. *Annu. Rev. Immunol.* **32**, 227–255 (2014).
- M. Canavese, F. Altruda, T. Ruzicka, J. Schaub, Vascular endothelial growth factor (VEGF) in the pathogenesis of psoriasis—A possible target for novel therapies? *J. Dermatol. Sci.* **58**, 171–176 (2010).
- Z. Wang, W. Liang, B. Zhang, M. Lv, J. Wang, L. Zhang, Single nucleotide polymorphisms of VEGF gene and psoriasis risk. *J. Dermatol. Sci.* **49**, 263–265 (2008).
- A. Datta-Mitra, N. K. Riar, S. P. Raychaudhuri, Remission of psoriasis and psoriatic arthritis during bevacizumab therapy for renal cell cancer. *Indian J. Dermatol.* **59**, 632 (2014).
- H. B. Schonhaler, J. Guinea-Viniegra, S. K. Wculek, I. Ruppen, P. Ximénez-Embún, A. Guío-Carrión, R. Navarro, N. Hogg, K. Ashman, E. F. Wagner, S100A8-S100A9 protein complex mediates psoriasis by regulating the expression of complement factor C3. *Immunity* **39**, 1171–1181 (2013).
- C. Halin, H. Fahrngruber, J. G. Meingassner, G. Bold, A. Littlewood-Evans, A. Stuetz, M. Detmar, Inhibition of chronic and acute skin inflammation by treatment with a vascular endothelial growth factor receptor tyrosine kinase inhibitor. *Am. J. Pathol.* **173**, 265–277 (2008).
- Y.-P. Xia, B. Li, D. Hylton, M. Detmar, G. D. Yancopoulos, J. S. Rudge, Transgenic delivery of VEGF to mouse skin leads to an inflammatory condition resembling human psoriasis. *Blood* **102**, 161–168 (2003).
- M. Detmar, The role of VEGF and thrombospondins in skin angiogenesis. *J. Dermatol. Sci.* **24** Suppl. 1, S78–S84 (2000).
- M. Detmar, L. F. Brown, M. P. Schön, B. M. Elicker, P. Velasco, L. Richard, D. Fukumura, W. Monsky, K. P. Claffey, R. K. Jain, Increased microvascular density and enhanced leukocyte rolling and adhesion in the skin of VEGF transgenic mice. *J. Invest. Dermatol.* **111**, 1–6 (1998).
- N. Ferrara, H.-P. Gerber, J. LeCouter, The biology of VEGF and its receptors. *Nat. Med.* **9**, 669–676 (2003).
- S. Koch, L. A. van Meeteren, E. Morin, C. Testini, S. Weström, H. Björkelund, S. Le Jan, J. Adler, P. Berger, L. Claesson-Welsh, NRP1 presented in trans to the endothelium arrests VEGFR2 endocytosis, preventing angiogenic signaling and tumor initiation. *Dev. Cell* **28**, 633–646 (2014).
- J. Yao, X. Wu, G. Zhuang, I. M. Kasman, T. Vogt, V. Phan, M. Shibuya, N. Ferrara, C. Bais, Expression of a functional VEGFR-1 in tumor cells is a major determinant of anti-PIGF antibodies efficacy. *Proc. Natl. Acad. Sci. U.S.A.* **108**, 11590–11595 (2011).
- B. Beck, G. Driessens, S. Goossens, K. K. Youssef, A. Kuchnio, A. Caauwe, P. A. Sotiropoulou, S. Loges, G. Lapouge, A. Candi, G. Mascré, B. Drogat, S. Dekoninck, J. J. Haigh, P. Carmeliet, C. Blanpain, A vascular niche and a VEGF-Nrp1 loop regulate the initiation and stemness of skin tumours. *Nature* **478**, 399–403 (2011).
- B. M. Lichtenberger, P. K. Tan, H. Niederleithner, N. Ferrara, P. Petzelbauer, M. Sibilia, Autocrine VEGF signaling synergizes with EGFR in tumor cells to promote epithelial cancer development. *Cell* **140**, 268–279 (2010).
- R. Zenz, R. Eferl, L. Kenner, L. Florin, L. Hummerich, D. Mehic, H. Scheuch, P. Angel, E. Tschachler, E. F. Wagner, Psoriasis-like skin disease and arthritis caused by inducible epidermal deletion of Jun proteins. *Nature* **437**, 369–375 (2005).
- A. Henno, S. Blacher, C. A. Lambert, C. Deroanne, A. Noël, C. Lapière, M. de la Brassinne, B. V. Nusgens, A. Colige, Histological and transcriptional study of angiogenesis and lymphangiogenesis in uninvolved skin, acute pinpoint lesions and established psoriasis plaques: An approach of vascular development chronology in psoriasis. *J. Dermatol. Sci.* **57**, 162–169 (2010).
- F. Shalaby, J. Ho, W. L. Stanford, K.-D. Fischer, A. C. Schuh, L. Schwartz, A. Bernstein, J. Rossant, A requirement for Flk1 in primitive and definitive hematopoiesis and vasculogenesis. *Cell* **89**, 981–990 (1997).
- H. K. Lee, S. K. Chauhan, E. Kay, R. Dana, Flt-1 regulates vascular endothelial cell migration via a protein tyrosine kinase-7-dependent pathway. *Blood* **117**, 5762–5771 (2011).
- A. Fantin, J. M. Vieira, A. Plein, L. Denti, M. Fruttiger, J. W. Pollard, C. Ruhrberg, NRP1 acts cell autonomously in endothelium to promote tip cell function during sprouting angiogenesis. *Blood* **121**, 2352–2362 (2013).
- B. Barleon, S. Sozzani, D. Zhou, H. A. Weich, A. Mantovani, D. Marme, Migration of human monocytes in response to vascular endothelial growth factor (VEGF) is mediated via the VEGF receptor flt-1. *Blood* **87**, 3336–3343 (1996).
- T. A. Wilgus, A. M. Matthies, K. A. Radek, J. V. Dovi, A. L. Burns, R. Shankar, L. A. DiPietro, Novel function for vascular endothelial growth factor receptor-1 on epidermal keratinocytes. *Am. J. Pathol.* **167**, 1257–1266 (2005).
- X.-Y. Man, X.-H. Yang, S.-Q. Cai, Z.-Y. Bu, M. Zheng, Overexpression of vascular endothelial growth factor (VEGF) receptors on keratinocytes in psoriasis: Regulated by calcium independent of VEGF. *J. Cell. Mol. Med.* **12**, 649–660 (2008).
- M. Canavese, F. Altruda, L. Silengo, V. Castiglioni, E. Scanziani, E. Radaelli, Clinical, pathological and immunological features of psoriatic-like lesions affecting keratin 14-vascular endothelial growth factor transgenic mice. *Histol. Histopathol.* **26**, 285–296 (2011).
- A. M. Jubb, L. A. Strickland, S. D. Liu, J. Mak, M. Schmidt, H. Koepfen, Neurophilin-1 expression in cancer and development. *J. Pathol.* **226**, 50–60 (2012).
- Q. Pan, Y. Chanthery, W.-C. Liang, S. Stawicki, J. Mak, N. Rathore, R. K. Tong, J. Kowalski, S. F. Yee, G. Pacheco, S. Ross, Z. Cheng, J. Le Couter, G. Plowman, F. Peale, A. W. Koch, Y. Wu, A. Bagri, M. Tessier-Lavigne, R. J. Watts, Blocking neurophilin-1 function has an additive effect with anti-VEGF to inhibit tumor growth. *Cancer Cell* **11**, 53–67 (2007).
- E. F. Wagner, H. B. Schonhaler, J. Guinea-Viniegra, E. Tschachler, Psoriasis: What we have learned from mouse models. *Nat. Rev. Rheumatol.* **6**, 704–714 (2010).

28. J. D. Buenrostro, P. G. Giresi, L. C. Zaba, H. Y. Chang, W. J. Greenleaf, Transposition of native chromatin for fast and sensitive epigenomic profiling of open chromatin, DNA-binding proteins and nucleosome position. *Nat. Methods* **10**, 1213–1218 (2013).
29. C. Bais, X. Wu, J. Yao, S. Yang, Y. Crawford, K. McCutcheon, C. Tan, G. Kolumam, J.-M. Verne, J. Eastham-Anderson, P. Haughney, M. Kowanz, T. Hagenbeek, I. Kasman, H. B. Reslan, J. Ross, N. Van Bruggen, R. A. D. Carano, Y.-J. G. Meng, J.-A. Hongo, J.-P. Stephan, M. Shibuya, N. Ferrara, PlGF blockade does not inhibit angiogenesis during primary tumor growth. *Cell* **141**, 166–177 (2010).
30. M. Keshtgarpour, A. Z. Dudek, SU-011248, a vascular endothelial growth factor receptor-tyrosine kinase inhibitor, controls chronic psoriasis. *Transl. Res.* **149**, 103–106 (2007).
31. S. Narayanan, K. Callis-Duffin, J. Batten, N. Agarwal, Improvement of psoriasis during sunitinib therapy for renal cell carcinoma. *Am. J. Med. Sci.* **339**, 580–581 (2010).
32. K. Jung, D. Lee, H. S. Lim, S.-I. Lee, Y. J. Kim, G. M. Lee, S. C. Kim, G. Y. Koh, Double anti-angiogenic and anti-inflammatory protein Valpha targeting VEGF-A and TNF- α in retinopathy and psoriasis. *J. Biol. Chem.* **286**, 14410–14418 (2011).
33. R. Kunstfeld, S. Hirakawa, Y.-K. Hong, V. Schacht, B. Lange-Asschenfeldt, P. Velasco, C. Lin, E. Fiebiger, X. Wei, Y. Wu, D. Hicklin, P. Bohlen, M. Detmar, Induction of cutaneous delayed-type hypersensitivity reactions in VEGF-A transgenic mice results in chronic skin inflammation associated with persistent lymphatic hyperplasia. *Blood* **104**, 1048–1057 (2004).
34. V. Vasioukhin, C. Bauer, L. Degenstein, B. Wise, E. Fuchs, Hyperproliferation and defects in epithelial polarity upon conditional ablation of α -catenin in skin. *Cell* **104**, 605–617 (2001).
35. C. Maes, S. Goossens, S. Bartunkova, B. Drogat, L. Coenegrachts, I. Stockmans, K. Moermans, O. Nyabi, K. Haigh, M. Naessens, L. Haenebalcke, J. P. Tuckermann, M. Tjwa, P. Carmeliet, V. Mandic, J. P. David, A. Behrens, A. Nagy, G. Carmeliet, J. J. Haigh, Increased skeletal VEGF enhances β -catenin activity and results in excessively ossified bones. *EMBO J.* **29**, 424–441 (2010).
36. C. Gu, E. R. Rodriguez, D. V. Reimert, T. Shu, B. Fritzs, L. J. Richards, A. L. Kolodkin, D. D. Ginty, Neuropilin-1 conveys semaphorin and VEGF signaling during neural and cardiovascular development. *Dev. Cell* **5**, 45–57 (2003).
37. B. K. Ambati, M. Nozaki, N. Singh, A. Takeda, P. D. Jani, T. Suthar, R. J. C. Albuquerque, E. Richter, E. Sakurai, M. T. Newcomb, M. E. Kleinman, R. B. Caldwell, Q. Lin, Y. Ogura, A. Orecchia, D. A. Samuelson, D. W. Agnew, J. St. Leger, W. R. Green, P. J. Mahasreshthi, D. T. Curiel, D. Kwan, H. Marsh, S. Ikeda, L. J. Leiper, J. M. Collinson, S. Bogdanovich, T. S. Khurana, M. Shibuya, M. E. Baldwin, N. Ferrara, H.-P. Gerber, S. De Falco, J. Witt, J. Z. Baffi, B. J. Raisler, J. Ambati, Corneal avascularity is due to soluble VEGF receptor-1. *Nature* **443**, 993–997 (2006).
38. H. Li, B. Handsaker, A. Wysoker, T. Fennell, J. Ruan, N. Homer, G. Marth, G. Abecasis, R. Durbin; 1000 Genome Project Data Processing Subgroup, The Sequence Alignment/Map format and SAMtools. *Bioinformatics* **25**, 2078–2079 (2009).

Acknowledgments: We thank the ULB animal facility and ULB genomic core facility. We thank F. Willaert and N. Cuyllits for providing human samples. **Funding:** F.B. was supported by the Fond Erasme. B.S. is supported by the FNRS. Y.S. is supported by the TELEVIE. C.B. is supported by the WELBIO, FNRS, ULB Foundation, the Foundation Baillet Latour, and the European Research Council (EXPAND). M.S. is supported by grants from the Austrian Science Fund (FWF, PhD program W1212 “Inflammation and Immunity”), the European Research Council (ERC) Advanced grant (ERC-2015-AdG TNT-Tumors 694883), the WWTF-project LS16-025, and the European Union’s Horizon 2020 research and innovation program under the Marie Skłodowska-Curie grant agreement no. 766214 (Meta-Can). **Author contributions:** C.B. and F.B. designed the experiments and performed the data analysis. F.B. performed most of the experiments. E.G. and M.S. designed and performed the experiments in the *c-Jun/JunB* psoriasis model. A.B., B.S., and Y.S. performed the bioinformatics analysis. V.d.M. cosupervised the study. M.R. and C.P. provided technical support. C.D. performed FACS isolation. C.B. and F.B. wrote the manuscript. **Competing interests:** The authors have no competing interests. **Data and materials availability:** All data needed to evaluate the conclusions in the paper are present in the paper and/or the Supplementary Materials. Additional data related to this paper may be requested from the authors.

Submitted 5 April 2019
Accepted 11 November 2019
Published 8 January 2020
10.1126/sciadv.aax5849

Citation: F. Benhadou, E. Giltzner, A. Brisebarre, B. Swedlund, Y. Song, C. Dubois, M. Rozzi, C. Paulissen, V. del Marmol, M. Sibilia, C. Blanpain, Epidermal autonomous VEGFA/Flt1/Nrp1 functions mediate psoriasis-like disease. *Sci. Adv.* **6**, eaax5849 (2020).

Epidermal autonomous VEGFA/Flt1/Nrp1 functions mediate psoriasis-like disease

Farida Benhadou, Elisabeth Glitzner, Audrey Brisebarre, Benjamin Swedlund, Yura Song, Christine Dubois, Milena Rozzi, Catherine Paulissen, Veronique del Marmol, Maria Sibilía and Cédric Blanpain

Sci Adv 6 (2), eaax5849.
DOI: 10.1126/sciadv.aax5849

ARTICLE TOOLS	http://advances.sciencemag.org/content/6/2/eaax5849
SUPPLEMENTARY MATERIALS	http://advances.sciencemag.org/content/suppl/2020/01/06/6.2.eaax5849.DC1
REFERENCES	This article cites 38 articles, 9 of which you can access for free http://advances.sciencemag.org/content/6/2/eaax5849#BIBL
PERMISSIONS	http://www.sciencemag.org/help/reprints-and-permissions

Use of this article is subject to the [Terms of Service](#)

Science Advances (ISSN 2375-2548) is published by the American Association for the Advancement of Science, 1200 New York Avenue NW, Washington, DC 20005. The title *Science Advances* is a registered trademark of AAAS.

Copyright © 2020 The Authors, some rights reserved; exclusive licensee American Association for the Advancement of Science. No claim to original U.S. Government Works. Distributed under a Creative Commons Attribution NonCommercial License 4.0 (CC BY-NC).